SUPPORTING INFORMATION

for

Reaction pathways and deactivation mechanisms of isostructural Cr and Fe MIL-101 during liquid-phase styrene oxidation by hydrogen peroxide

Rachel A. Yang[1] and Michele L. Sarazen[1,*]

[1]*Princeton University, Princeton, New Jersey 08540 (United States)*
Corresponding author: Michele L. Sarazen (msarazen@princeton.edu)

Keywords: metal-organic framework, aryl alkenes, oxidation, hydrogen peroxide, deactivation, mechanism

Table of Contents

Supporting information 2

Textural characterization 2

Figure S1 (Raw product images) 2
Figure S2 (Long range XRD patterns) 2
Figure S3 (Crystal size distribution) 2
Figure S4 (Cr phases crystal size distribution) 3
Figure S5 (Cr phases EDXS spectra, mapping) 3
Figure S6 (MIL-101(Fe) EDXS spectra, mapping) 3
Figure S7 (MIL-101(Fe) N_2 physisorption isotherms, PSDs) 4
Figure S8 (Post reaction N_2 physisorption isotherms, PSDs) 5
Figure S9 (Post reaction XRD patterns) 5
Figure S10 (FT-IR spectra for neat CH_3CN exposure at 323 K) 6
Figure S11 (Post reaction UV-Vis of Cr phase supernatants) 6
Figure S12 (NH_3-TPD) 7
Figure S13 (CO_2-TPD) 8
Figure S14 (MIL-53(Cr) unit cell, simulated XRD pattern) 9

^{1}H NMR spectra 9

Figure S15 (MIL-101(Fe) ^{1}H NMR at 353 K) 9
Figure S16 (^{1}H NMR of leached BDC linker) 10

Batch kinetic experiments 10

Figure S17 (MIL-101(Cr) hot filtration, 50 mg scale) 10
Figure S18 (MIL-101(Cr) hot filtration, 200 mg scale) 11
Figure S19 (MIL-101(Fe) hot filtration, 50 mg scale) 11
Figure S20 (MIL-101(Fe) hot filtration, 200 mg scale) 12

References 13

Supporting information

Textural characterization

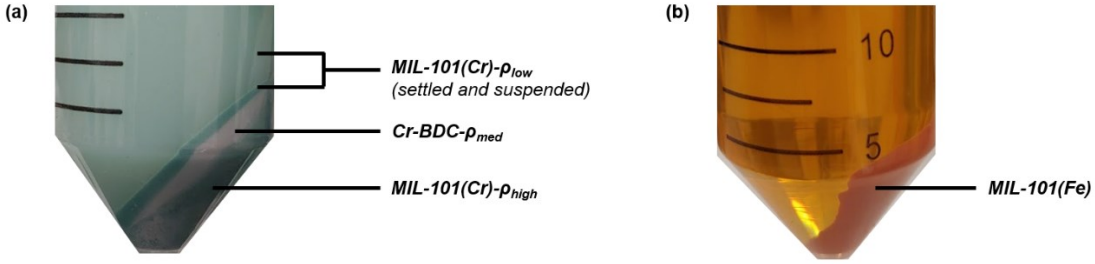

Figure S1 Raw products of (a) MIL-101(Cr) with MIL-101(Cr)-ρ_{high}, Cr-BDC-ρ_{med}, and MIL-101(Cr)-ρ_{low} phases and (b) MIL-101(Fe) after centrifugation (5000×g, 10 min.).

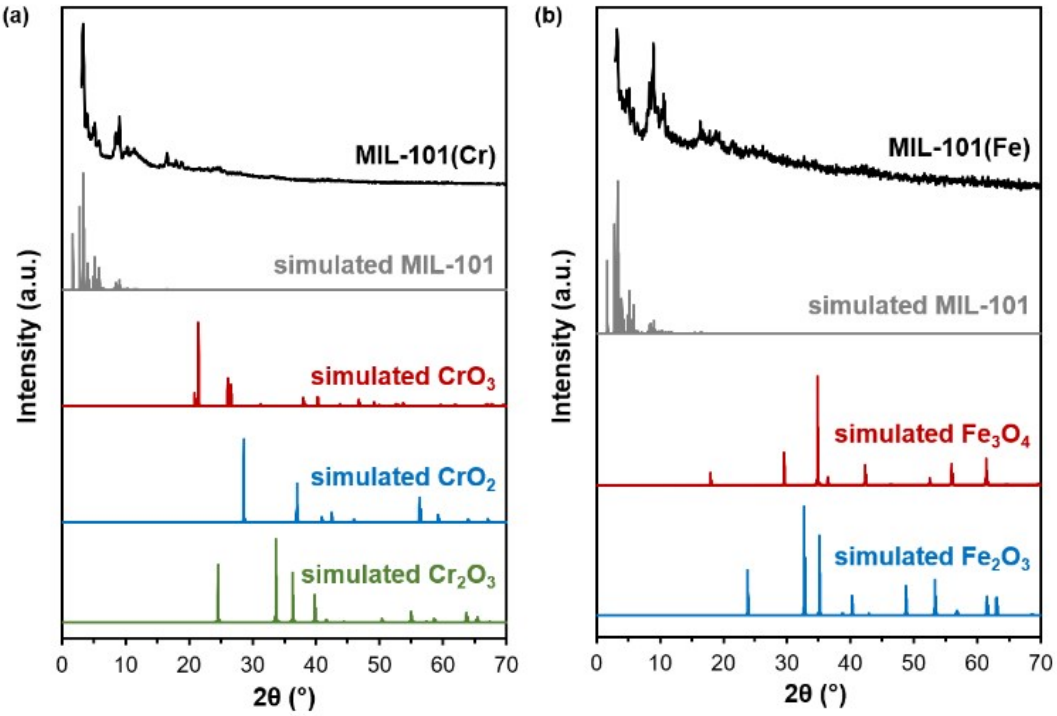

Figure S2 Long range XRD patterns of (a) MIL-101(Cr) (black) accompanied by simulated MIL-101 (grey), CrO_3 (red), CrO_2 (blue), and Cr_2O_3 (green) and (b) MIL-101(Fe) (black) accompanied by simulated MIL-101 (grey), Fe_3O_4 (red), and Fe_2O_3 (blue).

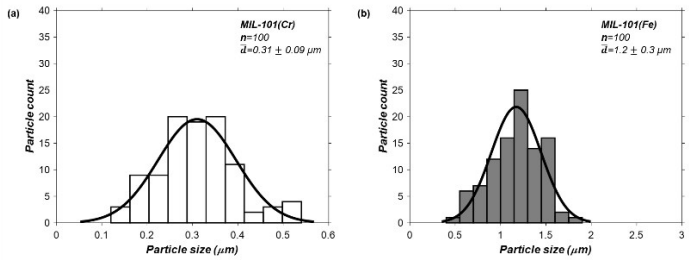

Figure S3 Particle diameter distributions for **n** particles from SEM images for (a) MIL-101(Cr) and (b) MIL-101(Fe).

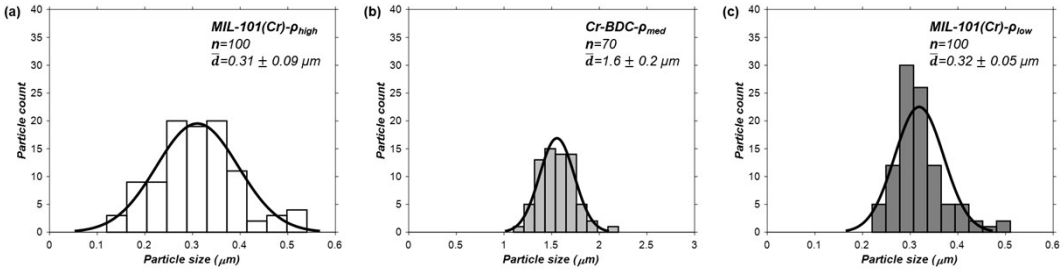

Figure S4 Particle diameter distributions for **n** particles from SEM images for (a) MIL-101(Cr)-ρ_{high} (white), (b) Cr-BDC-ρ_{med} (light grey), and (c) MIL-101(Cr)-ρ_{low} (dark grey).

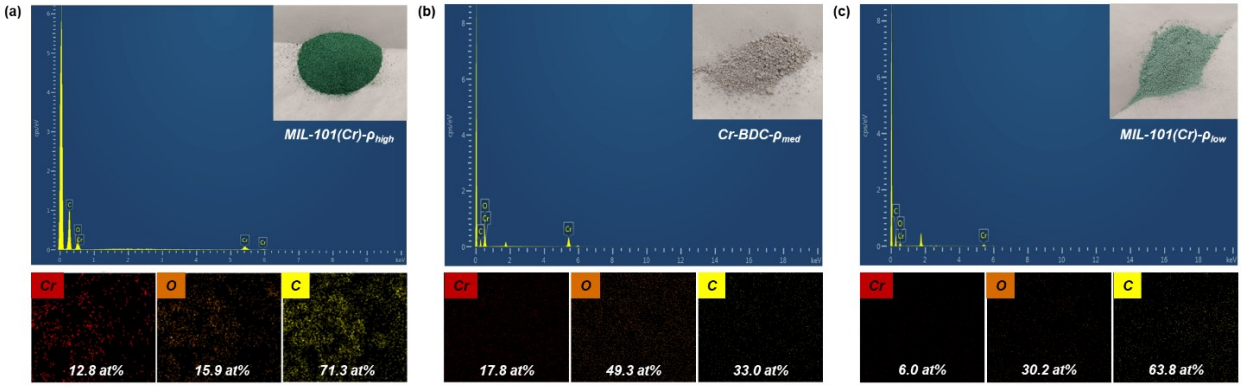

Figure S5 EDXS spectra and elemental mapping for fresh (a) MIL-101(Cr)-ρ_{high}, (b) Cr-BDC-ρ_{med}, and (c) MIL-101(Cr)-ρ_{low}. Insets are pictures of each phase.

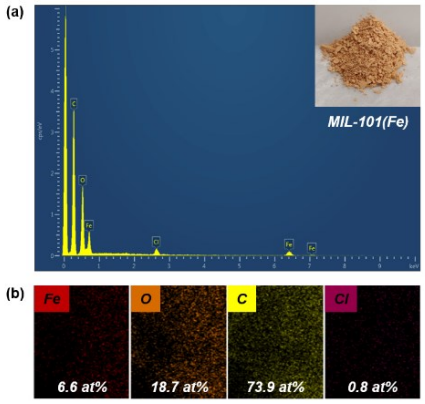

Figure S6 (a) EDXS spectra and (b) elemental mapping for fresh MIL-101(Fe). Inset is a picture of dried MIL-101(Fe).

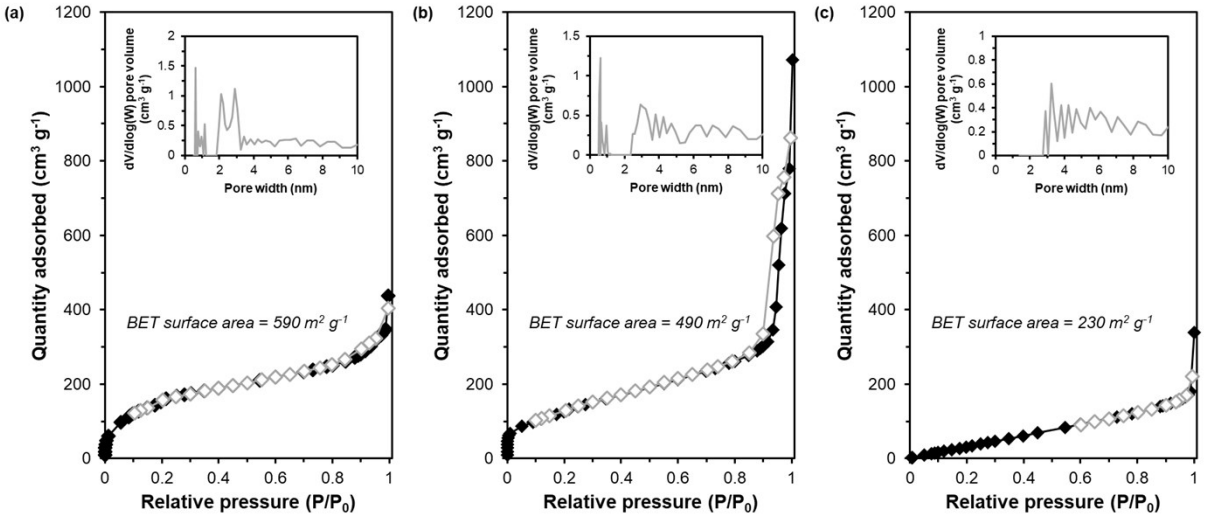

Figure S7 N_2 adsorption (black filled circles) and desorption (open grey diamonds) isotherms at 77 K and NLDFT PSDs (inset) for (a) high BET surface area (>500 m^2 g^{-1}), (b) intermediate BET surface area (300 m^2 g^{-1}<x<500 m^2 g^{-1}), and (c) low BET surface area (<300 m^2 g^{-1}) MIL-101(Fe).

Figure S7 shows obtained N_2 adsorption and desorption isotherms (77 K) for MIL-101(Fe) of varying BET surface areas. For clarification, we note that these samples were synthesized using the same protocol but were subjected to differing degassing procedures to determine operating parameters that do not induce degradation of the MIL-101(Fe) framework. The high (**Fig. S7a**) and low (**Fig. S7c**) BET surface area MIL-101(Fe) samples were degassed at 313 K for 2 days at 125 torr while the intermediate BET surface area sample (**Fig. S7b**) was degassed at 383 K overnight at 125 torr. As mentioned in the main text, purification, thermal activation, and degassing procedures may all contribute to the measured BET surface area for MIL-101(Fe) so it is still unclear which factors contribute most significantly.

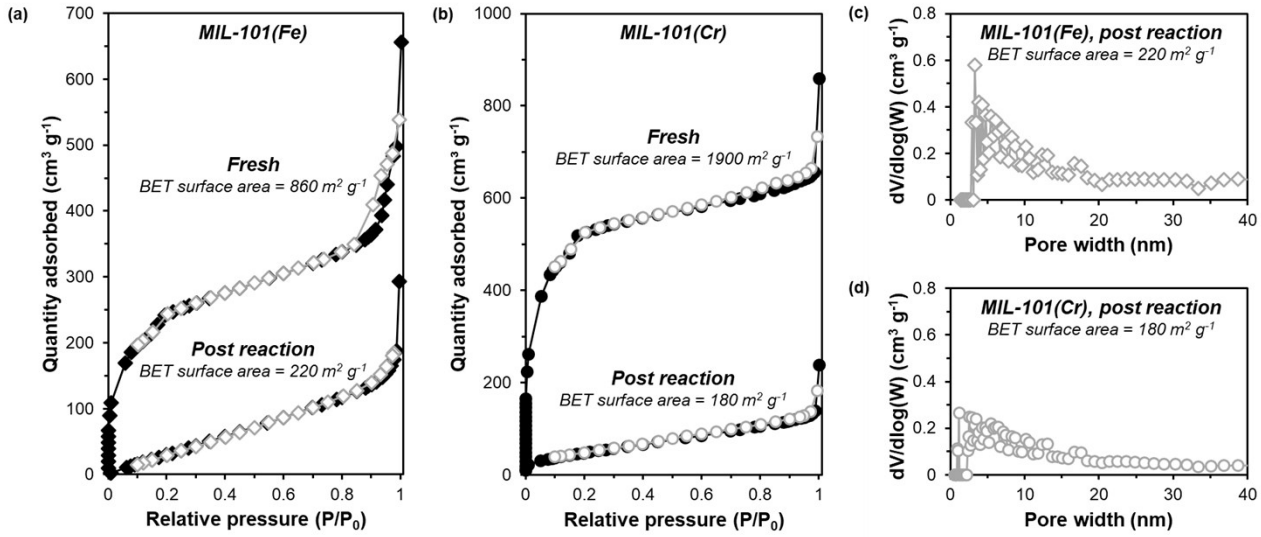

Figure S8 N_2 adsorption (black filled) and desorption (open grey) isotherms at 77 K for (a) fresh and post reaction high BET surface area (>500 m^2 g^{-1}) MIL-101(Fe) and (b) fresh and post reaction MIL-101(Cr) with post reaction referring to styrene oxidation by hydrogen peroxide at 323 K (3600 s). NLDFT PSD for (c) post reaction MIL-101(Fe) and (d) post reaction MIL-101(Cr). Reaction broth was scaled up to 200 mg catalyst, 40 mL CH_3CN, 40 mmol styrene, and 120 mmol hydrogen peroxide but reflect the same concentrations as batch experiments (50 mg catalysts, 10 mL CH_3CN, 10 mmol styrene, 30 mmol hydrogen peroxide) described in the main text.

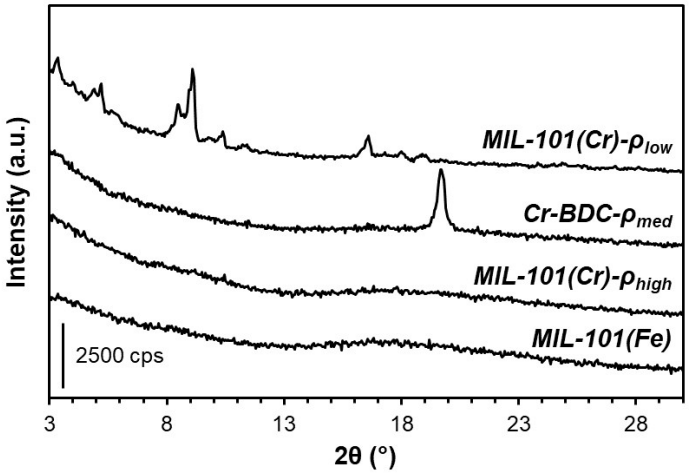

Figure S9 XRD patterns of MIL-101(Fe), MIL-101(Cr)-ρ_{high}, Cr-BDC-ρ_{med}, MIL-101(Cr)-ρ_{low} after reaction at 323 K, 3600 s. Samples were reactivated by washing with acetonitrile and ethanol sequentially and then drying under vacuum (125 torr) overnight.

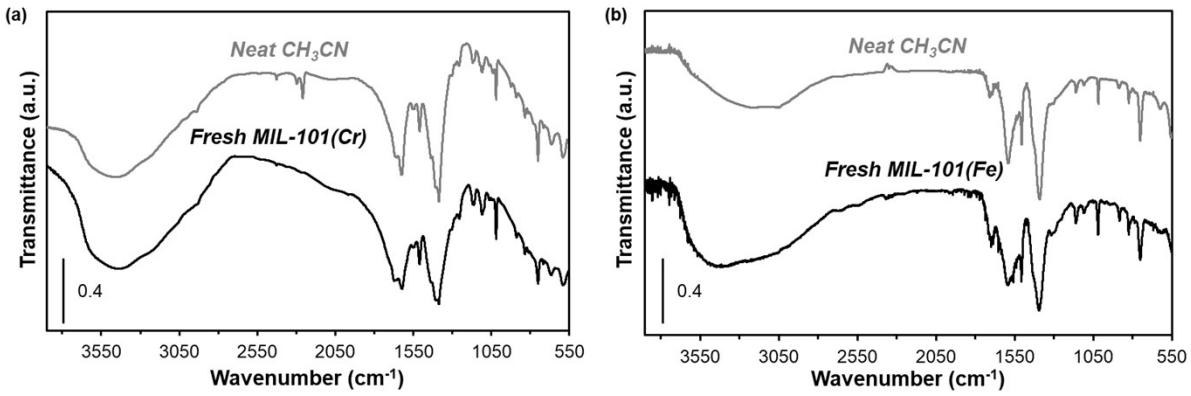

Figure S10 FTIR spectra of fresh and spent catalysts after 3600 s at 323 K in neat CH_3CN for (a) MIL-101(Cr) and (b) MIL-101(Fe).

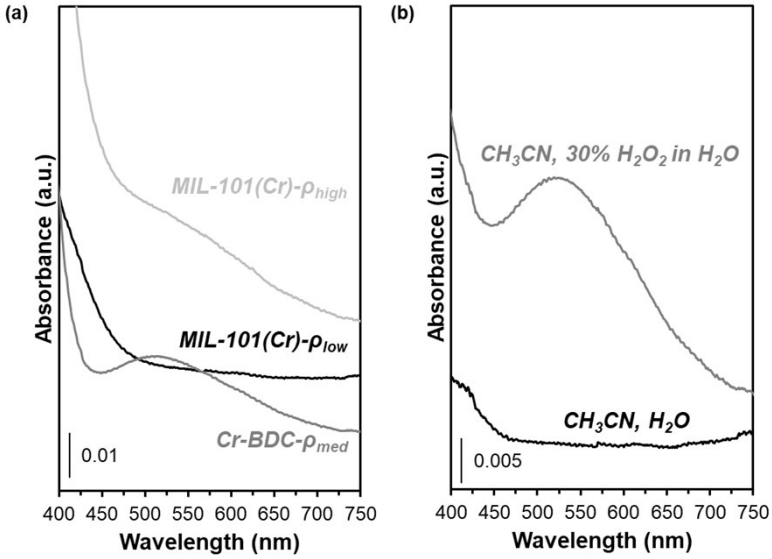

Figure S11 UV-Vis spectra of (a) reaction broths after hot filtration tests for MIL-101(Cr)-ρ_{high} (light grey), Cr-BDC-ρ_{med} (dark grey), and MIL-101(Cr)-ρ_{low} (black) and (b) filtrate after 3600 s stability tests at 323 K in neat CH_3CN+H_2O (black) and CH_3CN+30% H_2O_2 in H_2O (grey) for MIL-101(Cr)-ρ_{high}.

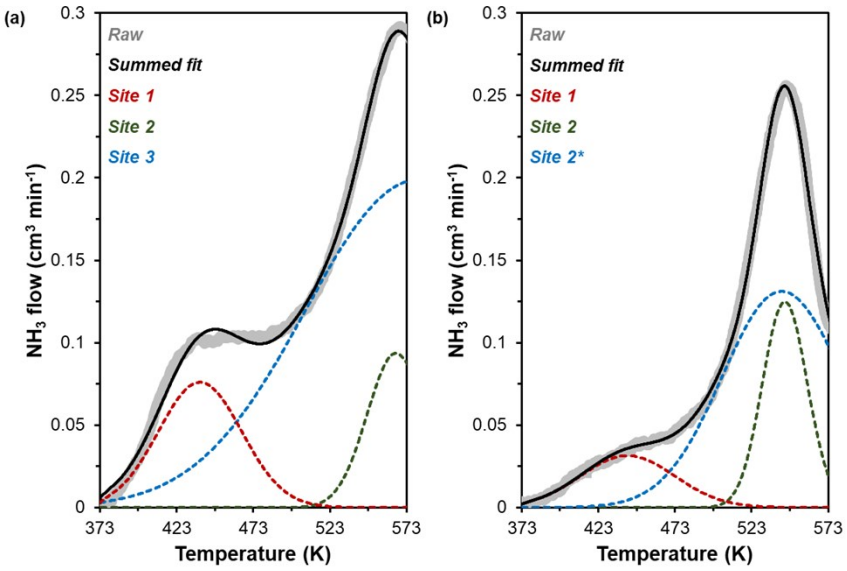

Figure S12 NH_3-TPD for (a) MIL-101(Fe) and (b) MIL-101(Cr) with fitted gaussian peaks.

NH_3-TPD experiments were performed on a Micromeritics Autochem II 2920. Samples (25-30 mg) were packed into a U-tube with a quartz wool plug underneath the catalyst bed. Water and volatile organics were baked off at 383 K for 2 h after ramping to temperature at 10 K min^{-1} under 30 mL min^{-1} helium flow. After cooling to 373 K, 30 mL min^{-1} of 10% NH_3 in helium was flowed over the catalyst bed for 2 h. Helium (30 mL min^{-1}) was then flowed to purge the sample and U-tube of excess NH_3 for 1 h. After a stable baseline (TCD signal) was achieved, the temperature was ramped at 5 K min^{-1} to 773 K with a measurement taken every second to generate the profiles in **Figure S12**. Finally, samples were cooled back to ambient temperature under helium and discarded.

Raw NH_3-TPD profiles were baseline corrected by subtracting a profile for a U-tube containing only the quartz wool plug obtained under the same experimental conditions. Afterwards, Fityk software was used to fit Gaussian distributions. The centers of these fitted distributions informed reported site strengths (desorption temperature) and the areas gave site densities of each site. Error associated with fitting each Gaussian was reported in the main text. We note that for MIL-101(Cr) (**Fig. S12b**), site 2 and site 2* were both needed to obtain decent agreement between the summed fit and the raw data. However, it is unlikely that these two peaks represent distinct sites and are instead combined to represent Cr(III) sites. For MIL-101(Fe), there is precedent in other iron carboxylate MOFs that both Fe(II) and Fe(III) sites exist,[1,2] so these two sites (site 2 and site 3) were reported separately.

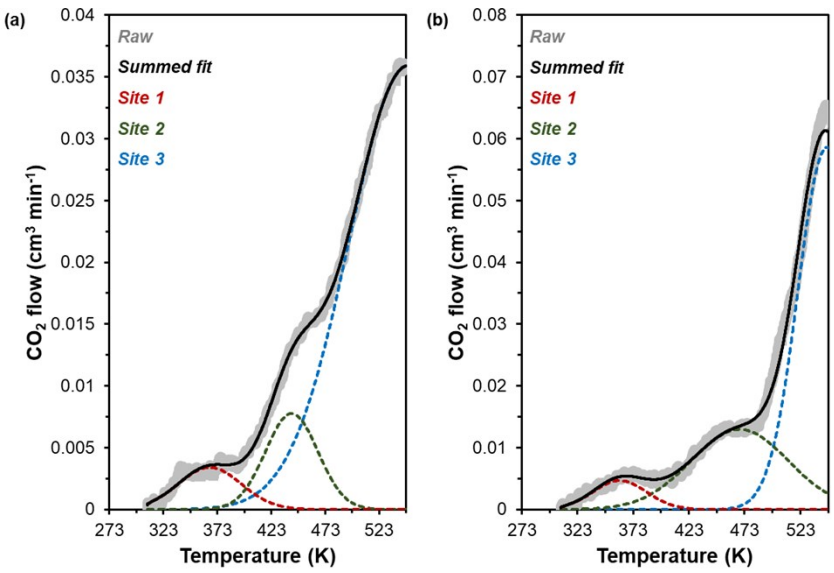

Figure S13 CO_2-TPD for (a) MIL-101(Fe) and (b) MIL-101(Cr) with fitted gaussian peaks.

CO_2-TPD experiments were also performed on a Micromeritics Autochem II 2920 in a similar manner as NH_3-TPD experiments. A glass U-tube was packed with a quartz wool plug and sample masses on the order of 30 mg. Under a 30 mL min^{-1} helium flow, water and other volatile components were removed at 383 K for 2 h after ramping to temperature at 10 K min^{-1}. The bed was cooled to 308 K and then 30 mL min^{-1} of 10% CO_2 in helium was flowed over the catalyst bed for 1 h. To purge to sample and U-tube of excess CO_2, 30 mL min^{-1} of helium was then flowed for 1 h. After a stable TCD signal was acquired, the temperature was ramped at 5 K min^{-1} to 773 K with a measurement taken every second to produce the profiles in **Figure S13**. The samples were cooled under helium to ambient temperature and then discarded.

Similar to NH_3-TPD profiles, the baseline CO_2-TPD profile for a U-tube containing a quartz plug was subtracted from the raw CO_2-TPD profiles obtained for MIL-101(Cr) and MIL-101(Fe). Fityk was used to fit Gaussian distributions and the analysis of desorption temperature and site densities was also applied for these profiles. Associated error with these fits is reported in the main text and were determined in the same manner as for NH_3-TPD.

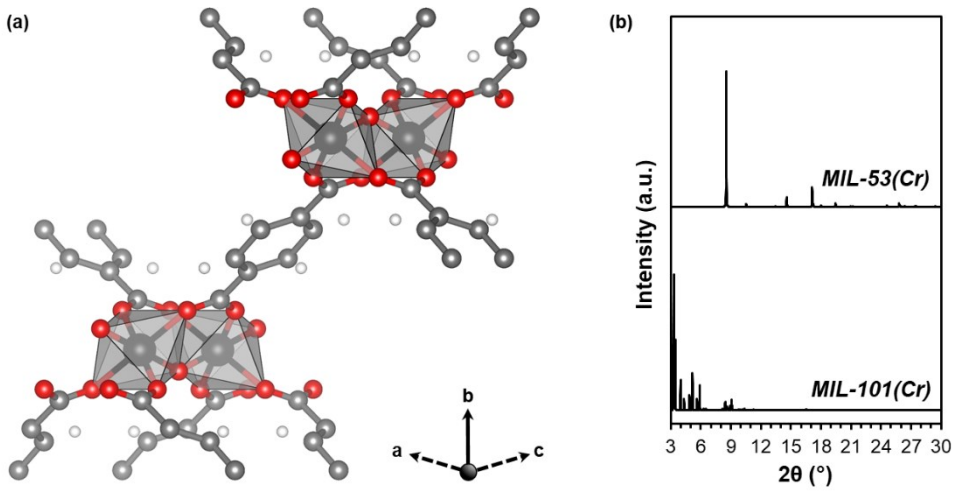

Figure S14 (a) Unit cell for MIL-53(Cr). (b) XRD patterns for simulated MIL-53(Cr) and MIL-101(Cr).

^{1}H NMR spectra

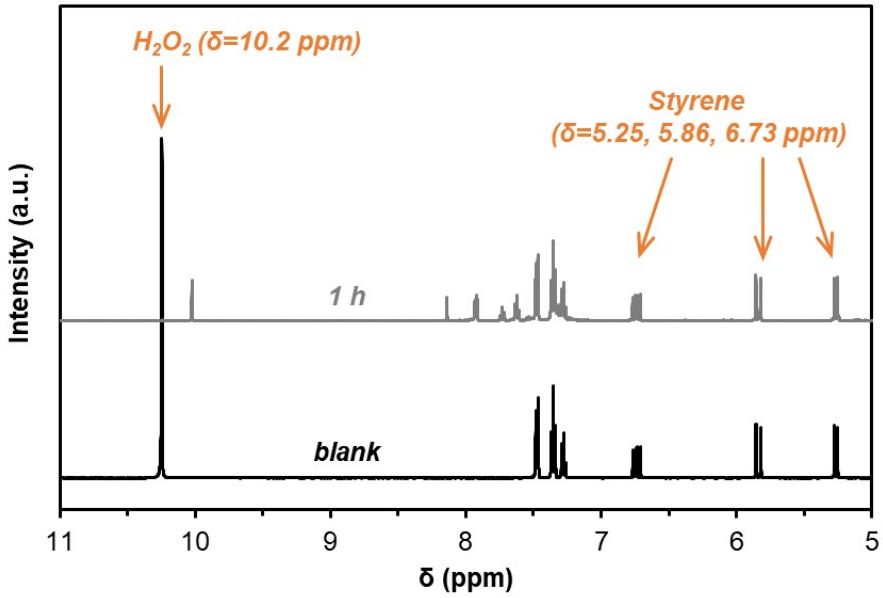

Figure S15 ^{1}H-NMR for reaction broth before catalyst introduction (blank; black) and of 3600 s timepoint for Fe (grey) at elevated temperature (353 K). Spectra are stacked for clarity.

Initial studies attempting to mirror existing literature cycling experiments at 353 K[3] resulted in observations that decomposition of hydrogen peroxide to gaseous products overwhelmingly dominates on the Fe framework, evidenced by vigorous bubbling in the reaction broth and a singlet peak reduction at 10.2 ppm corresponding to hydrogen peroxide coincident with relatively unchanged styrene peak intensities observed in ^{1}H NMR spectra after 3600 s (**Fig. S15**). From this, it is apparent that at 353 K, Cr and Fe have significantly different pathway preferences, with the Cr analog being able to turnover oxygenate products and the Fe analog preferring hydrogen peroxide decomposition. Thus, no reliable comparison could be drawn between Fe and Cr styrene oxidation reactivity at this higher temperature.

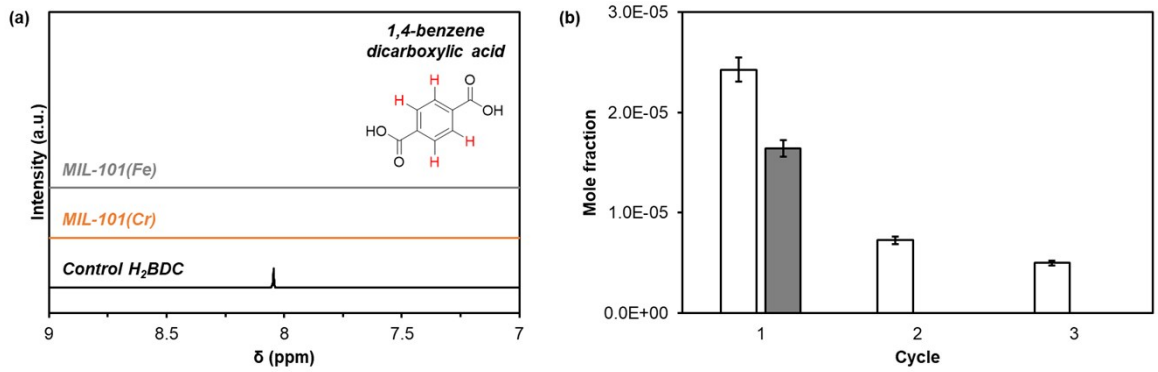

Figure S16 (a) ^{1}H NMR spectra of H_2BDC (black) and filtrate after MIL-101(Cr) (red) and MIL-101(Fe) (grey) were exposed to neat CH_3CN for 3600 s at 323 K. (b) Mole fractions of leached H_2BDC for each cycle over MIL-101(Cr) (white) and MIL-101(Fe) (grey).

Batch kinetic experiments

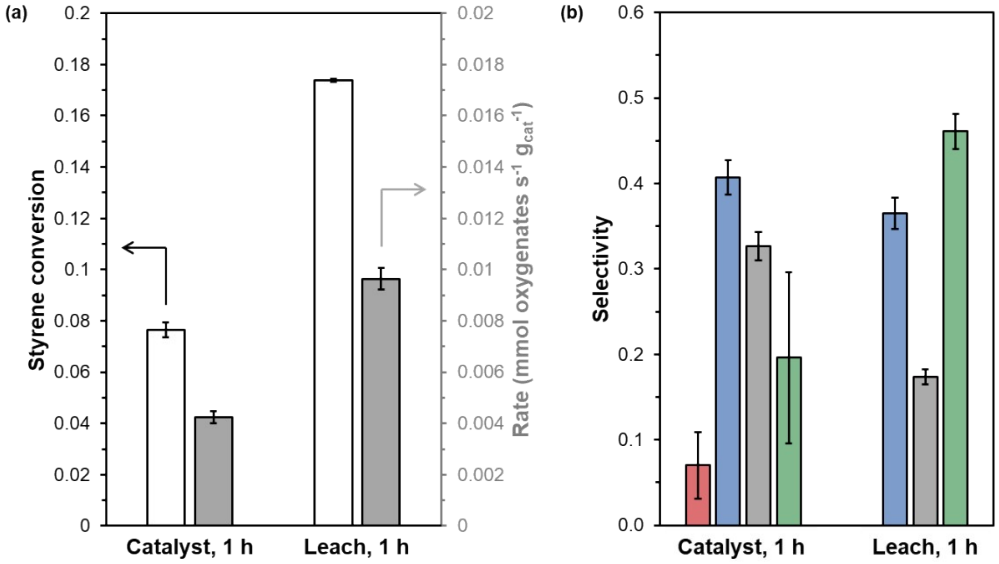

Figure S17 (a) Styrene conversion (white) and oxygenate production turnover rates at 3600 s (grey) for MIL-101(Cr) at 323 K. (b) Oxygenate (styrene oxide (red), benzaldehyde (blue), styrene glycol (grey), benzoic acid (green)) selectivities at 3600 s. Reaction broth composition: 50 mg catalyst, 10 mL CH_3CN, 10 mmol styrene, 30 mmol H_2O_2.

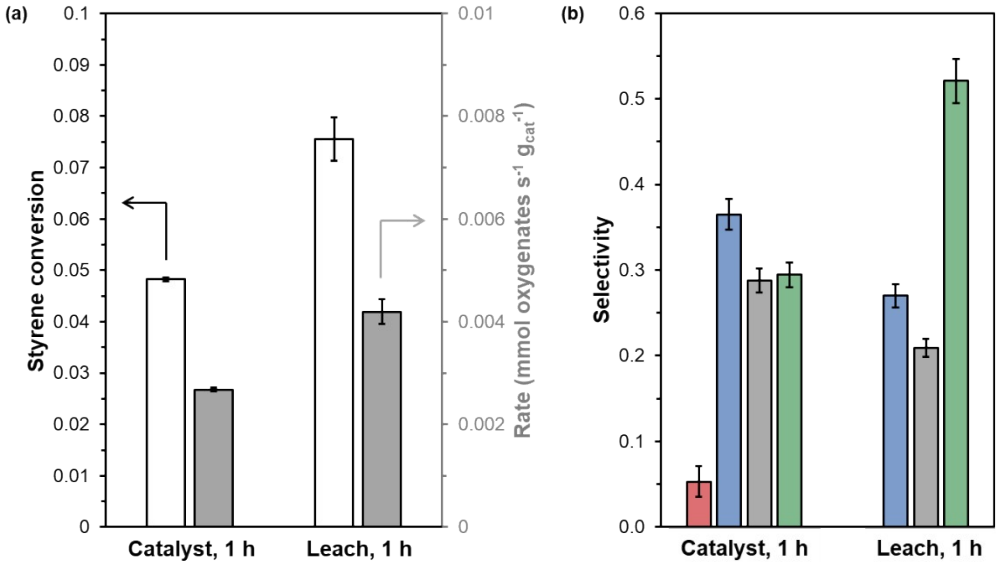

Figure S18 (a) Styrene conversion (white) and oxygenate production turnover rates at 3600 s (grey) for MIL-101(Cr) at 323 K. (b) Oxygenate (styrene oxide (red), benzaldehyde (blue), styrene glycol (grey), benzoic acid (green)) selectivities at 3600 s. Reaction broth composition: 200 mg catalyst, 40 mL CH_3CN, 40 mmol styrene, 120 mmol H_2O_2.

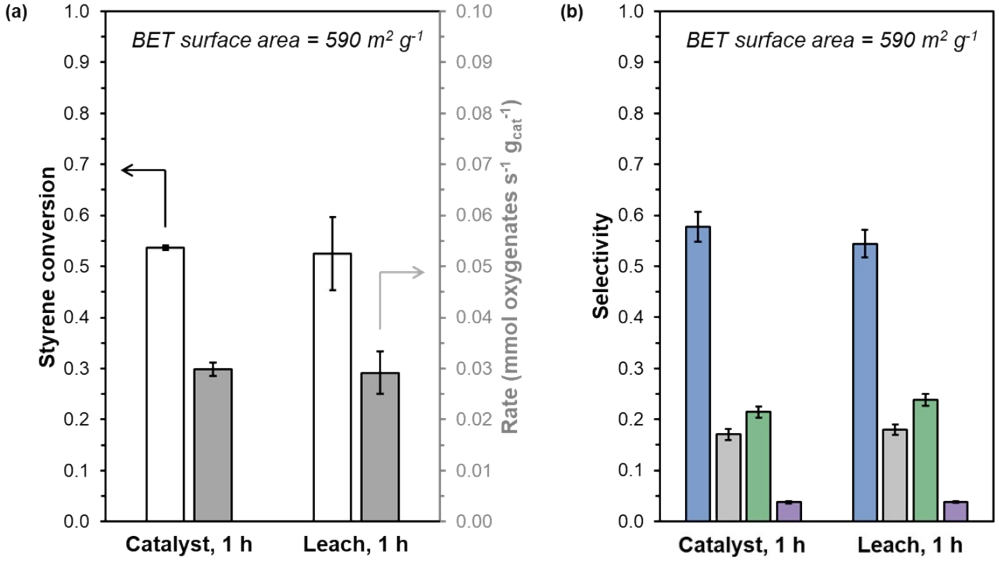

Figure S19 (a) Styrene conversion (white) and oxygenate production turnover rates at 3600 s (grey) for "lower surface area" MIL-101(Fe) (590±10 m^2 g^{-1}) at 323 K. (b) Oxygenate (benzaldehyde (blue), styrene glycol (grey), benzoic acid (green), phenylacetaldehyde (purple)) selectivities at 3600 s. Reaction broth composition: 50 mg catalyst, 10 mL CH_3CN, 10 mmol styrene, 30 mmol H_2O_2.

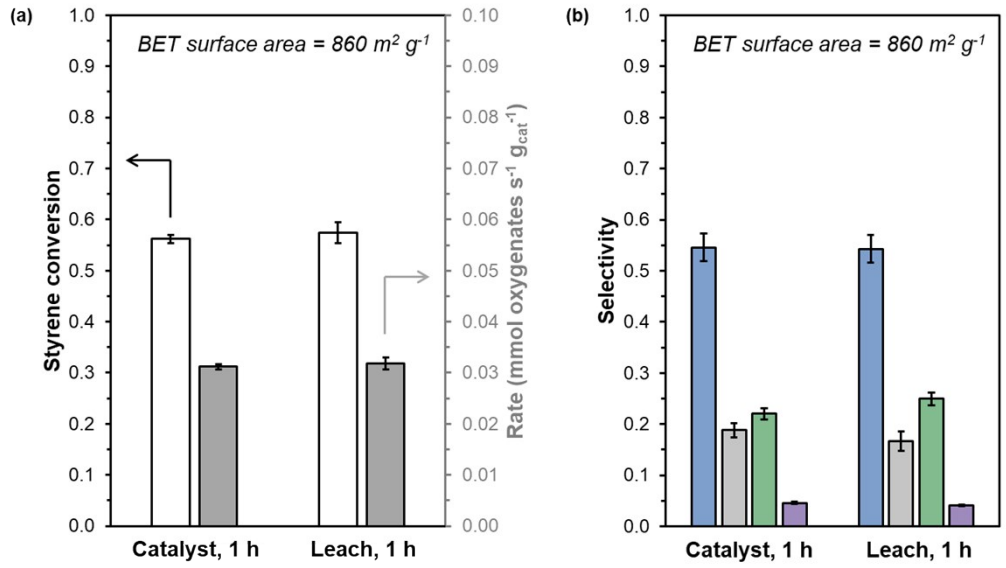

Figure S20 (a) Styrene conversion (white) and oxygenate production turnover rates at 3600 s (grey) for "higher surface area" MIL-101(Fe) (860±10 m^2 g^{-1}) at 323 K. (b) Oxygenate (benzaldehyde (blue), styrene glycol (grey), benzoic acid (green), phenylacetaldehyde (purple)) selectivities at 3600 s. Reaction broth composition: 200 mg catalyst, 40 mL CH_3CN, 40 mmol styrene, 120 mmol H_2O_2.

The hot filtration experiments for MIL-101(Cr)-ρ_{high} (**Fig. S17, S18**) and MIL-101(Fe) (**Fig. S19, S20**) were done on a different catalyst batches than those used in cycling experiments reported in the main text due to limited yields from small-scale syntheses. **Figures S17** and **S19** were conducted using an initial charge of 50 mg catalyst, 10 mL CH_3CN, 10 mmol styrene, and 30 mmol H_2O_2 while **Figures S18** and **S20** are scaled up by a factor of 4 (200 mg catalyst, 40 mL CH_3CN, 40 mmol styrene, 120 mmol H_2O_2) to recover enough solid after reaction for N_2 physisorption experiments.

For MIL-101(Cr)-ρ_{high}, the oxygenate production rate normalized by moles of metal on these batches (**Fig. S17:** 6.30±0.36 mM oxygenates s^{-1} mmol Cr^{-1}, **Fig. S18:** 3.31±0.05 mM oxygenates s^{-1} mmol Cr^{-1}) is on the same order of magnitude as that reported in the main text (4.23±0.25 mM oxygenates s^{-1} mmol Cr^{-1}). Oxygenate product distribution in these batches, however, differs slightly from that in **Figure 5c**. These batches show a 31.4% (**Fig. 17**) and 48.0 % (**Fig. S18**) lower styrene oxide selectivity than that reported in **Figure 5c**, though this is consistent with higher defect densities in these batches, as evidenced by a lower Cr loading from EDXS. Despite this, the hot filtration test confirms that leached Cr species are active and impact both styrene conversion and product distribution.

For MIL-101(Fe), the mass-normalized oxygenate production rate for these batches (**Fig. S19:** 2.21±0.10 mM oxygenates $g_{catalyst}^{-1}$ s^{-1}, **Fig. S20:** 2.31±0.18 mM oxygenates $g_{catalyst}^{-1}$) is effectively identical to that in **Figure 5** (1.97±0.10 mM oxygenates $g_{catalyst}^{-1}$ s^{-1}). However, these batches show small fractional selectivity for phenylacetaldehyde (**Fig. S19:** 0.037±0.001, **Fig. S20:** 0.046±0.001) whereas no phenylacetaldehyde is observed in **Figure 5d**. Despite this difference in product distribution for this batch, no styrene oxide is observed and product ordering is still largely consistent between these samples and that used for cycling experiments (benzaldehyde > benzoic acid > styrene glycol > phenylacetaldehyde). Further, these hot filtration experiments for MIL-101(Fe) demonstrates that neither styrene conversion nor product

distribution changes after the solid catalyst is removed, indicating that observed catalytic activity is heterogeneous in nature.

References

1 A. Dhakshinamoorthy, M. Alvaro, P. Horcajada, E. Gibson, M. Vishnuvarthan, A. Vimont, J. M. Grenèche, C. Serre, M. Daturi and H. Garcia, *ACS Catal.*, 2012, **2**, 2060–2065.

2 M. Pu, Y. Ma, J. Wan, Y. Wang, J. Wang and M. L. Brusseau, *Catal. Sci. Technol.*, 2017, **7**, 1129–1140.

3 J. Sun, G. Yu, Q. Huo, Q. Kan and J. Guan, *RSC Adv.*, 2014, **4**, 38048–38054.